scientific reports

Check for updates

OPEN

Distinct alterations in white matter properties and organization related to maternal treatment initiation in neonates exposed to HIV but uninfected

Ndivhuwo Magondo[1,2]✉, Ernesta M. Meintjes[1,2,7]✉, Fleur L. Warton[1,2], Francesca Little[3], Andre J. W. van der Kouwe[1,4,5], Barbara Laughton[6], Marcin Jankiewicz[1,2,7,9] & Martha J. Holmes[1,2,8,9]

HIV exposed-uninfected (HEU) infants and children are at risk of developmental delays as compared to HIV uninfected unexposed (HUU) populations. The effects of exposure to in utero HIV and ART regimens on the HEU the developing brain are not well understood. In a cohort of 2-week-old newborns, we used diffusion tensor imaging (DTI) tractography and graph theory to examine the influence of HIV and ART exposure in utero on neonate white matter integrity and organisation. The cohort included HEU infants born to mothers who started ART before conception (HEU_{pre}) and after conception (HEU_{post}), as well as HUU infants from the same community. We investigated HIV exposure and ART duration group differences in DTI metrics (fractional anisotropy (FA) and mean diffusivity (MD)) and graph measures across white matter. We found increased MD in white matter connections involving the thalamus and limbic system in the HEU_{pre} group compared to HUU. We further identified reduced nodal efficiency in the basal ganglia. Within the HEU_{post} group, we observed reduced FA in cortical-subcortical and cerebellar connections as well as decreased transitivity in the hindbrain area compared to HUU. Overall, our analysis demonstrated distinct alterations in white matter integrity related to the timing of maternal ART initiation that influence regional brain network properties.

The developing brain is at its most vulnerable in utero, where it depends on the maternal environment to provide nutrients and protection. Disruptions to the maternal ecosystem may occur as a result of viral, bacterial or parasitic infections. Studies have established that even indirect contact with a viral infection in utero can lead to adverse effects in fetuses, suggesting that the maternal immune response and symptoms of infections may contribute to adverse prenatal development[1,2]. While treatments for infection that may restore maternal health are available, such as antivirals and antibiotics, there may be negative neurodevelopmental consequences for the fetus[3,4].

HIV (human immunodeficiency virus) targets and alters the immune system. In women living with HIV, the virus can adversely affect maternal health as well as fetal development. During pregnancy, antiretroviral therapy (ART) provides protection to the fetus by preventing HIV proliferation in the mother, allowing her immune system to strengthen. Due to increased availability of ART, the rate of vertical HIV transmission has decreased

[1]Division of Biomedical Engineering, Department of Human Biology, Faculty of Health Sciences, Biomedical Engineering Research Centre, University of Cape Town, Cape Town, South Africa. [2]Neuroscience Institute, University of Cape Town, Cape Town, South Africa. [3]Department of Statistical Sciences, University of Cape Town, Cape Town, South Africa. [4]A.A. Martinos Center for Biomedical Imaging, Massachusetts General Hospital, Charlestown, MA, USA. [5]Department of Radiology, Harvard Medical School, Boston, MI, USA. [6]Department of Paediatrics and Child Health and Tygerberg Children's Hospital, Faculty of Medicine and Health Sciences, Family Centre for Research with Ubuntu, Stellenbosch University, Stellenbosch, South Africa. [7]Cape Universities Body Imaging Centre, University of Cape Town, Cape Town, South Africa. [8]Department of Biomedical Physiology and Kinesiology, Simon Fraser University, Burnaby, BC, Canada. [9]ImageTech, Simon Fraser University, Surrey, BC, Canada. ✉email: ndi.magondo@uct.ac.za; ernesta.meintjes@uct.ac.za

substantially leading to a growing population of HIV exposed uninfected (HEU) infants. Although uninfected, HEU infants demonstrate higher risks of cognitive deficits, particularly in language and motor skills, compared to HIV unexposed uninfected (HUU) populations[5].

White matter connections play an integral role in cognition because they facilitate rapid transmission of information between different brain areas[6]. In utero, white matter organization primarily involves the development of axonal fibers. Axonal pathways start developing at 8 post conceptual weeks, the end of the embryonic stage, into the neonatal period. Pre-myelination begins in the second trimester as fibers mature and myelin forming cells develop. Mature myelin appears between 20 and 28 weeks of gestational age (GA), with the portion of total brain volume that contains myelinated white matter increasing from 1 to 5% between 36 and 40 weeks GA[7]. As a result, disruptions to the maternal environment across the stages of pregnancy can disrupt different aspects of developing white matter.

The basic structural and functional wiring of the brain is already in place at birth[6]. During the last trimester of pregnancy, short and long connections between brain regions develop to create an early adult-like organization of neural networks[8]. At birth, a large network of connections is already present, which may be referred to as a connectome[9]. Given the time sensitive nature of white matter development, the timing of ART initiation during pregnancy may contribute to its ability to provide protection or disruption of white matter development.

Diffusion tensor imaging (DTI) yields quantitative measures reflecting properties of white matter. Biological models of developing white matter in utero and early infancy based on imaging measures have been proposed from which typical white matter development, including axon growth/development, pre-myelination and myelination, can be inferred based on changes in DTI parameters[10].

While several publications have looked at the effects of HIV exposure on white matter in infants/children unexposed and living without HIV using DTI data[11–15], only one has used tractography[13]. Unlike other approaches, tractography estimates white matter properties within a pair of regions which provides anatomical context. It also allows for further study of the properties of connectivity between regions, using approaches such as graph analysis. While previous DTI studies report subtle exposure related regional differences in infants[15] and children[11–14], it isn't yet known if these disrupt structural organization. In addition, no DTI study has yet included the possible influence of timing of maternal ART treatment initiation on developing white matter.

The work presented identifies potential HIV and ART exposure differences in white matter connections and networks shortly after birth in a cohort of HEU and HUU newborns. We proposed that maternal ART protects developing white matter from the effects of maternal infection. We hypothesized infants born to mothers on treatment at conception would demonstrate white matter integrity similar to HUU infants, whereas HEU newborns exposed to ART post conception would have altered regional connectivity. Lastly, we posited regional connectivity changes would affect network properties.

Methods

Study cohort

The Healthy Baby Study (HBS) conducted in Cape Town, South Africa, included pregnant women living with and without HIV. The study enrolled 226 women, 18 years or older, at < 30 weeks' gestation. The group comprised 82 HIV-free women and 144 women living with HIV. Among pregnant women living with HIV who were recruited, approximately half initiated ART prior to conception ($n = 78$) and half initiated treatment post conception ($n = 66$). As part of standard care in South Africa, HIV status is confirmed at the antenatal clinic using an HIV Rapid test. If positive, pregnant women living with HIV start first line therapy Tenofovir (TDF), Emtricitabine (FTC) and Efavirenz (EFV) in a daily fixed dose combination. HIV viral load is assessed at a follow up visit.

Exclusion criteria were underlying chronic disorders (e.g., diabetes, epilepsy, tuberculosis, hypertension), a history of recurrent premature deliveries, tuberculosis contact, use of medication other than essential pregnancy supplements, Isoniazid preventative therapy, or ART (if living with HIV), and for those with HIV, poor adherence to ART, not being on fixed drug combination ART (TDF, FTC, EFV), or nondisclosure of HIV status to family members. Prior to enrolment, mothers were also interviewed regarding their alcohol and drug use habits using the timeline follow back questionnaire[16,17]. Mothers engaged in illicit drug use, binge drinking (4 or more drinks per occasion) or drinking more than minimally (> 7 drinks per week), were also excluded.

Pregnant women provided written informed consent for themselves and their infants to participate in the study. The HBS study was conducted in accordance with protocols approved by the Health Sciences Human Research Ethics Committees of Stellenbosch (ref: M16/10/041 and S21/11/231) and the University of Cape Town (ref: 801/2016).

Gestational age was determined by the study clinicians using date of Last Menstrual Period (LMP) and Ultrasound as per American College of Obstetrician and Gynaecologists (ACOG) (2017) guidelines[18]. If no ultrasound or accurate LMP was available, physical examination was used according to local guidelines[19].

For mothers living with HIV, HIV viral load (VL), CD4 count and treatment records were obtained throughout pregnancy at antenatal visits.

For prevention of vertical transmission, infants born to women living with HIV were given Nevirapine if considered low risk. Infants at high risk of vertical transmission, defined as a maternal VL > 1000 copies/mL at 32 weeks GA, are also prescribed Zidovudine. Infants were excluded if they were born earlier than 36 weeks GA, weighed less than 2500 g at birth, received a positive HIV-1 PCR test, or were diagnosed with a condition that could influence neurodevelopment. Further details about the maternal and infant inclusion and exclusion criteria can be found in Ibrahim et al.[20].

Infants born to mothers living with HIV who initiated ART before conception are referred to as HEU preconception, or HEU_{pre}. Similarly, neonates born to mothers living with HIV who started ART during pregnancy, are denoted as HEU post-conception, or HEU_{post}.

MRI acquisition

The study performed brain imaging on neonates using a 3T Siemens Skyra MRI scanner (Siemens, Erlangen, Germany) at the Cape Universities Body Imaging Centre (CUBIC) located at Groote Schuur Hospital. Prior to scanning, newborns had their diapers changed and were tightly swaddled to reduce motion. Sponge ear plugs and specially designed foam ear pads were placed in and over their ears, held in place by a beanie cap. The infants were fed and put to sleep in supine position on a special styrofoam bead pillow in a 16-channel paediatric head coil (Siemens), and imaged without sedation.

The protocol included a high-resolution T1-weighted (T1w) 3D echo-planar imaging (EPI) navigated multi-echo magnetization-prepared rapid gradient-echo (MEMPRAGE) acquisition (FOV 192×192 mm^2, TR 2540 ms, TI 1450 ms, TEs = 1.69/3.55/5.41/7.27 ms, BW 650 Hz/px, 144 sagittal slices, voxel size $1.0 \times 1.0 \times 1.0$ mm^3). Two diffusion-weighted imaging (DWI) sets with opposite (Anterior–Posterior, Posterior-Anterior; AP/PA) phase encoding directions were acquired with a multi-band[21] twice refocused spin-echo EPI sequence: TR 4800 ms, TE 84 ms, matrix 62 axial slices of 96×96 voxels (each voxel $2 \times 2 \times 2$ mm^3), 6/8 partial Fourier encoding, BW 1628 Hz/px, with slice-acceleration factor 2 and GRAPPA factor 2. Each acquisition contained six b = 0 s/mm^2 (b0) reference scans and 30 DW gradient directions with b = 1000 s/mm^2.

Image processing

All analyses were carried out using a combination of predeveloped in-house scripts and tools available in standard software packages such as the Analysis of Functional Neuroimages (AFNI) toolbox[22], the Tolerably Obsessive Registration and Tensor Optimisation Indolent Software Ensemble (TORTOISE) version 3.1.0[23], Infant Freesurfer[24], and the Functional And Tractographic Connectivity Analysis Toolbox (FATCAT)[25] within AFNI.

(AFNI)'s *fat_proc_imit2w_from_t1w* function was used to create T2-weighted (T2w) anatomical image imitation of the T1w structural image. Next, each subject's DW images were quality checked across both AP and PA directions. Subjects with less than 15 (50%) viable diffusion directions (out of the 30 present) and/or no viable b0 images (out of the 6) were excluded from further analyses. After exclusions, the DIFF_PREP function in TORTOISE was used to correct for DWI artefacts such as motion and eddy current distortions. The DRBUDDI function combined the AP and PA directions to perform EPI distortion correction and created a final set of DW images for each subject[26]. AFNI's *fat_proc_dwi_to_dt* function was used to estimate diffusion tensors and DTI parameters.

Regions of interest (ROIs) were extracted from T1w images using Infant Freesurfer version 4a14499, which uses an automated algorithm to segment the infant brain[24,27]. Infant FreeSurfer segments each hemisphere into 8 subcortical ROIs, lateral-, 3rd- and 4th ventricles, cerebral and cerebellar cortex, and cerebral white matter, as well as 4 medial structures, namely vermis, midbrain, pons and medulla. The left and right hemispheric cerebral white matter were not included as seeds in our analyses. We included the ventricles because of their location relative to subcortical structures. The third ventricle is between the right and the left thalamus, while the fourth ventricle sits within the brainstem, at the intersection between the pons and medulla oblongata. The final set of DW images were co-registered to Tw1 images to map the seeds to the DWI space.

DTI and tractography

The diffusion metrics commonly extracted in DTI analysis include mean diffusivity (MD), fractional anisotropy (FA), axial diffusivity (AD) and radial diffusivity (RD). MD reflects the average amount of water diffusion within a voxel[28]. It is lower in regions of high tissue complexity as this creates diffusion obstacles[28], and is typically low within white matter due to the large number of axonal connections present[28]. However, in infant brains, MD is often significantly higher than in mature adult brains because brain water content decreases during maturation[28]. In infant brains, the majority of axons are unmyelinated and structures such as cell and axonal membranes are less densely packed, so water is more readily able to diffuse perpendicularly. FA is used as an index of the amount of anisotropy within a specified region[29]. In tissue, FA describes the directional coherence of diffusivity and for this reason is used as a quantitative marker of white matter integrity[28]. The degree of anisotropy is associated with axon density and axon count, and while the degree of myelination relates to FA as well, it does not define tissue anisotropy.

AD, also known as longitudinal or parallel diffusion, refers to diffusivity on the principal axis of the diffusion ellipsoid. RD, also known as transverse or perpendicular diffusion, refers to diffusivity perpendicular to the principal direction of the diffusion ellipsoid, or an average of diffusion along the ellipsoid's two minor axes[28]. Low AD is typically associated with axonal damage and fragmentation, while RD has been related to fiber coherence, myelin integrity, axonal diameter, and axonal density[28]. Presenting AD and RD can be helpful for interpretation, as changes in AD and RD typically drive changes in FA[30,31].

Biological changes specific to the developing brain have been linked to DTI parameters[8]. The following Table 1 summarizes the changes in white matter in pre-term and term infants.

Tractography was performed between every pair of seeds using FATCAT (version 1.1)[25] in AFNI. The *3dTrackID* function was used to perform fully probabilistic tractography[32]. The stopping criteria for this study included the following: angle threshold (turning angle > 60°), FA threshold for infants (FA < 0.1) and tract length (< 20 mm)[33,34].

The outputs of the 3dTrackID are a set of the following measures—FA, MD, AD, RD, bundle length (BL), number of voxels in a bundle (NV), fractional volume of the bundle (fNV) and fractional number of streamlines in a given tract (fNT)—for each tract connecting the ROIs and subject. Due to inter-subject variability of data, sets of tracts for each subject could in principle be different. To ensure a common subset of tracts and DTI measures among the entire population in the study, we used the intersection of all the individual sets of tracts.

FA	MD	AD	RD	Biological interpretation
↑	–	↑	↓	Axonal fasciculation
–	↓	↓	↓	Pre-myelination; proliferation of oligodendrocytes and membranes
↑	↓	–	↓	Myelination

Table 1. Summary of the changes in DTI parameters and their biological description in developing white matter.

Graph theory

Tractography parameters were used as inputs for graph theory analysis. We defined a graph as set of nodes (ROIs) and weighted edges (white matter tracts). The weight of each edge was defined by fNT.

Each subject's structural n x n connectivity matrix (n being number of nodes) weighted by connections' fNT gave rise to a weighted adjacency matrix for each subject. Graph analysis was performed using R statistical software[35] and the igraph package for brain network analysis. A mean graph was created for each group (HUU, HEU_{pre} and HEU_{post}) using the weighted adjacency matrices.

Graph theory, in the context of the WM connectome, provides quantitative measure of WM organization. Graph measures can be divided into three types based on brain function: brain network, segregation and integration.

Brain network measures describe features of brain connectivity. Nodal degree and strength are network measures describing white matter connectivity in terms of the number of connections to a seed region. Nodes with high nodal degree act as communication hubs[36]. Nodal strength increases as the brain develops, with lower strength linked to axonal damage in children[37,38].

Structural segregation represents the capacity for specialized processing within brain regions[36]. Modularity, clustering coefficient, transitivity (normalized clustering coefficient) and local efficiency are all metrics of segregation. These measures describe the brain's ability to engage in specialized processing. Decreased local efficiency has been linked to traumatic brain injury in children[37].

Structural integation describes the ability to combine information from different brain regions. Characteristic path length, nodal efficiency and global efficiency are integration measures. Path length decreases, while nodal and global efficiency increase, as the brain becomes better at processing information with age. Disruptions to integration measures have been linked to associative fiber damage[36].

A summary defining graph theory measures of interest and their potential biological interpretations is presented below in Table 2.

Graph measure	Measurement	Biological interpretation
Network measures (Connectivity)		
Nodal degree	White matter connectivity represented by the number of connections to a seed region.	Nodes with high degree act as communication hubs[36].
Nodal strength	A weighted measure of white matter connectivity given by the sum of white matter connections to a seed region.	Nodes with higher strength act as hubs of communication between more specialised and spatially constraint brain areas. Higher nodal strength represents stronger structural connectivity[39,40]. Nodal strength increases as the brain develops, with lower strength linked to axonal damage in children[37,38].
Segregation measures (Functional specialization)		
Modularity	A measure representing how much a network can be broken into smaller parts with high interconnectivity[41].	Modular networks are best adapted to tasks performed in a changing environment[41]. In children, modularity reduces with age as networks become more integrated and specialized.
Transitivity	The overall probability for the network to have adjacent nodes interconnected[41].	High transitivity indicates high levels of local organisation and densely interconnected groups in the network, which improves the brain's ability to do specialised processing[42]. Decreased transitivity may represent transitory myelin damage[43].
Local efficiency	Local efficiency characterises how well a node exchanges information with its neighbours when it is removed[44].	Higher local efficiency indicates better local integration[44]. Alterations in local efficiency may signify disruptions in neural communication or processing efficiency within specific nodes or brain regions, and has been linked to traumatic brain injury in children [37,44].
Integration measures (Information processing)		
Nodal efficiency	Measures nodal information exchange.	High nodal efficiency indicates effective information flow and connectivity to other nodes in the network[45]. Nodal efficiency increases with age as the ability to send information grows. Low nodal efficiency indicates lower information integration or processing efficiency.
Global efficiency	A measure of a network's parallel information processing efficiency[46].	Global efficiency increases with age as the network becomes more efficient.

Table 2. Graph theory measures and their clinical interpretations in brain networks.

Statistical analysis

Statistical analyses were performed using R statistical software[35]. We used linear regression models to compare the differences arising from HIV exposure and different maternal ART starting times (HUU vs HEU_{pre} and HEU_{post}) in both DTI and graph theory measures.

DTI measures of interest were extracted, and outliers were removed from every common pairwise connection between target ROIs. Outliers were identified as values less than 1.5 times the interquartile range (IQR) below the lower quartile ($Q_L - 1.5(IQR)$) or 1.5 times the IQR above the upper quartile ($Q_U + 1.5(IQR)$). The outliers in the analyses of graph theoretical measures were removed in an analogous fashion.

DTI measures were then used in linear regression models. To identify confounders, we summarised the likely associations between potential confounders (infant sex, gestational age equivalent at scan, weight at scan, head circumference at scan, maternal weight gain per week of pregnancy, maternal education, ounces absolute alcohol consumed per day across pregnancy (oz AA/day) and maternal age at delivery), exposure variables and imaging outcome variables.

For the linear regression models, we chose a statistical significance level of $p = 0.05$. Subsequently, we corrected the calculated p-values for multiple comparisons using the false discovery rate (FDR) method. The corrected p-values, presented as q-values, were deemed statistically significant at a level of $q < 0.05$.

To explore the possible influence of maternal immune health on affected white matter integrity and network measures, we performed correlation analysis between DTI outcome measures and maternal CD4 count in pregnancy within tracts and networks showing group differences.

Results

Sample demographics

After exclusions, 187 infants were enrolled in the study (67 HUU, 63 HEU_{pre}, 55 HEU_{post}), of whom 185 visited CUBIC for neonatal MRI (2 HEU_{pre} infants missed their scan). Of the 160 neonates who had T1 and DTI images, 108 had complete sets of DTI scans (satisfying the quality check conditions outlined in the "Methods" section). A further two infants were excluded due to poor quality T1 images, leaving 106 infants for the analysis.

The data included for analysis consisted of 35 HUU and 71 HEU (36 HEU_{pre}/35 HEU_{post}) infants. The sample demographics are presented in Table 3. The pre-conception HEU infant group was exposed to ART throughout

	HIV unexposed uninfected (HUU)	HIV exposed uninfected (HEU)	
		HEU_{pre}	HEU_{post}
Number of subjects (n)	35	36	35
Sex (Male: Female)	18:17	18:18	20:15
Birth measures			
Gestational age (weeks)	40 ± 1	40 ± 2	40 ± 2
Weight (g)	3285 ± 407	3215 ± 333	3250 ± 403
Length (cm)	50 ± 4	50 ± 2	50 ± 3
ARV exposure length (weeks)	N/A	40 ± 1	25 ± 6
MRI scan measures			
Age at scan (weeks)	1.9 ± 1	1.5 ± 1	1.8 ± 1
Gestational age equivalent (weeks)	42 ± 1	41 ± 1	42 ± 1
Weight (g)	3561 ± 439	3143 ± 411	3509 ± 379
Length (cm)	52 ± 2	51 ± 2	52 ± 2
Head circumference (cm)	35 ± 1	36 ± 1	35 ± 1
Maternal measures			
Birth age (years)	28 ± 6	31 ± 6	28 ± 5
CD4 count within 6 months of pregnancy (cells/mm^3)	N/A	571 ± 180	435 ± 194
Distribution of peak Viral Loads (VLs) during pregnancy (n, %)			
< 20 copies/mL	N/A	25 (69%)	18 (51%)
≥ 20–400 copies/mL	N/A	7 (19%)	11 (31%)
≥ 400–1000 copies/mL	N/A	2 (6%)	2 (6%)
≥ 1000 copies/mL	N/A	2 (6%)	4 (11%)
Detectable VL throughout pregnancy (n, %)	N/A	1 (3%)	10 (29%)
Weight gain per week (g)	0.41 ± 0.16	0.35 ± 0.28	0.27 ± 0.24
Ounces absolute alcohol per day (oz AA/day)[a]	0.02 ± 0.02	0.01 ± 0.02	0.02 ± 0.03

Table 3. Demographic data of HUU controls and HEU groups at birth and at time of MRI scanning. Mean and standard deviations (SD) presented as Mean ± SD. [a]1 oz AA ~ 2 standard drinks.

gestation, the infants in the HEU_{post} group were exposed to ART in utero between 14 and 36 weeks. Across infant growth measures, the groups were well matched.

DTI tractography

Figure 1 shows the 28 ROIs that were used as seeds in our analyses.

Before regression was run, full-probabilistic DTI tractography identified a total of 173 tracts between seeds to be common to all the subjects. For regression analysis, maternal weight gain per week of pregnancy and maternal education were included as confounding variables. Using these tracts and confounders, we report the tracts showing HIV and ART exposure-related differences DTI measurs.

Across all group comparisons, analysis of bundle length, total number of tracts, number of voxels in a bundle and fractional volume of the bundle yielded no statistically significant group differences.

Reduced FA and higher MD in HEU pre-conception infants

We observed group differences in both FA and MD when comparing the HEU_{pre} infants to their HUU peers. Table 4 summarizes the five tracts with reduced FA. All connections include the left cerebral cortex, with tracts to the midbrain and subcortical structures represented. Figure 2 presents chord diagram visualizing the significant conncections across DTI parameters.

As shown in Table 5, we find seventeen tracts with increased MD in the HEU pre-conception group as compared to HUU infants. Figure 2 shows approximately half (8 or 47%) involve the left or right thalamus. Within these tracts, we observe higher MD accompanied by higher AD and RD.

Reduced FA in HEU post-conception infants

In the HEU-post conception group we did not identify group differences in MD.

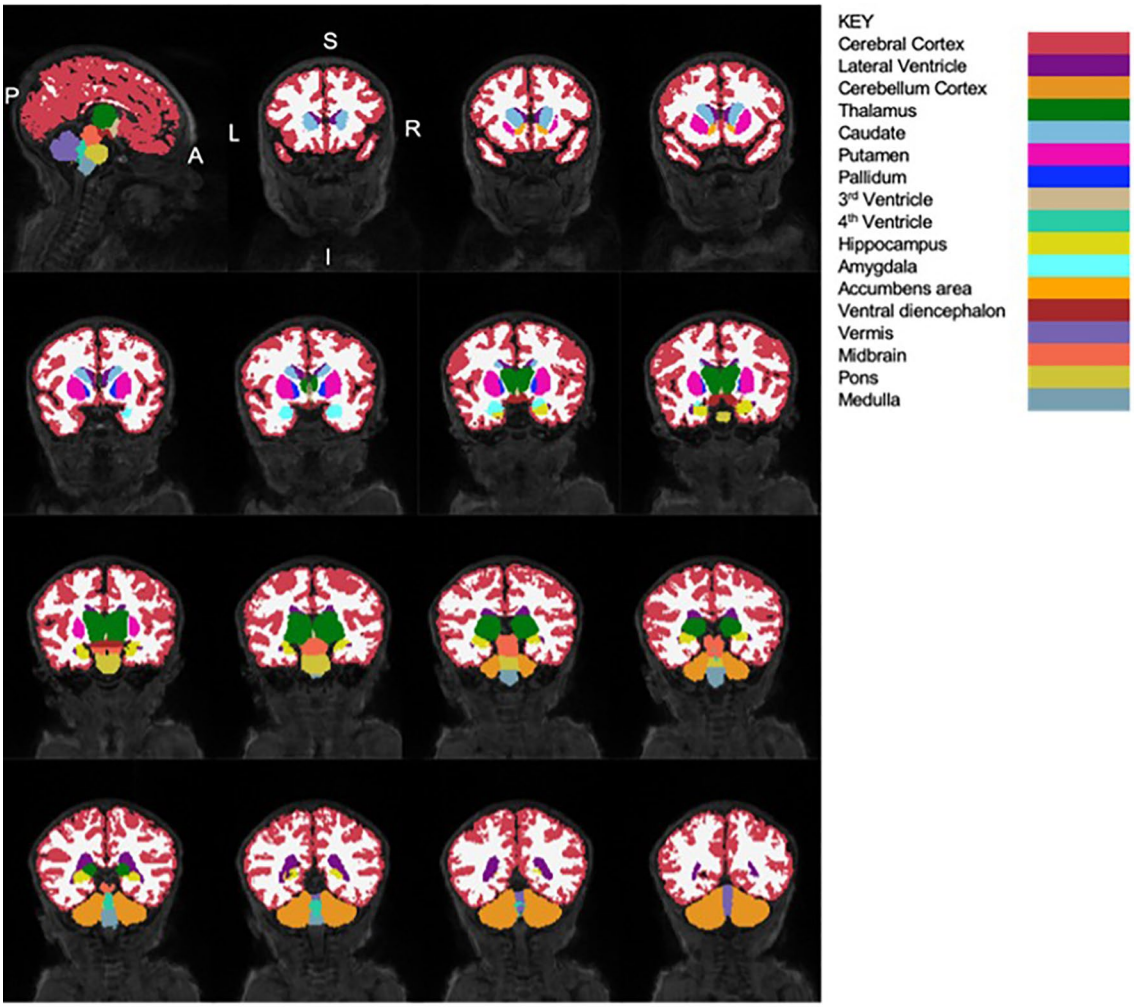

Figure 1. Sagittal and coronal views of neonatal brain (from a randomly selected HUU infant) showing the segmented structures and their corresponding labels (segmented in Infant Freesurfer). To visualise different structures, coronal slices are presented from the anterior to posterior direction. A/P, Anterior/Posterior; L/R, Left/Right; S/I, Superior/Inferior.

Connections	FA						AD						RD					
	Mean HUU (SD)	Mean HEU_{pre} (SD)	p	q	Std beta	Std error	Mean HUU (SD)	Mean HEU_{pre} (SD)	p	q	Std beta	Std error	Mean HUU (SD)	Mean HEU_{pre} (SD)	p	q	Std beta	Std error
L CC—L Caud	0.221 (0.007)	0.214 (0.009)	0.0006	0.036	− 0.479	0.137	1.633 (0.069)	1.630 (0.044)	0.990	0.990	− 0.002	0.016	1.172 (0.057)	1.181 (0.031)	0.379	0.456	0.126	0.132
L CC—L Put	0.208 (0.008)	0.200 (0.008)	0.0012	0.046	− 0.451	0.130	1.605 (0.063)	1.618 (0.051)	0.372	0.473	0.125	0.016	1.172 (0.060)	1.194 (0.047)	0.141	0.231	0.203	0.156
L CC—L VDC	0.224 (0.009)	0.216 (0.008)	0.0002	0.028	− 0.499	0.140	1.648 (0.061)	1.653 (0.061)	0.611	0.674	0.071	0.018	1.173 (0.058)	1.191 (0.051)	0.197	0.292	0.178	0.151
L CC—R Thal	0.235 (0.009)	0.228 (0.011)	0.0013	0.046	− 0.402	0.129	1.676 (0.078)	1.705 (0.058)	0.052	0.138	0.270	0.019	1.169 (0.054)	1.197 (0.046)	0.043	0.113	0.277	0.140
L CC—MB	0.225 (0.007)	0.219 (0.007)	0.0005	0.036	− 0.499	0.136	1.632 (0.062)	1.647 (0.061)	0.367	0.473	0.127	0.017	1.156 (0.050)	1.182 (0.046)	0.049	0.117	0.274	0.139

Table 4. Tracts showing lower fractional anisotropy (FA) in HEU_{pre} infants than HUU after FDR correction ($q < 0.05$). Axial diffusivity (AD) and radial diffusivity (RD) in affected tracts are also shown. SD, standard deviation; L/R, Left/Right hemisphere. CC, Cerebral Cortex; Caud, Caudate; Put, Putamen; VDC, Ventral Diencephalon; Thal, Thalamus; MB, Midbrain.

In Table 6 we present 28 white matter connections with lower mean FA in HEU infants born to mothers who initiated ART post conception relative to HUU infants. The chord diagrams in Fig. 3 show that all except 5 tracts involve connections to either the cerebral cortex or the cerebellum.

Within these results, we find no significant group differences in AD or RD after multiple comparisons. The uncorrected p-values suggest FA reductions in a subset of these connections are due to increased RD.

Reduced FA in HEU infants independent of ART initiation

Looking at Tables 4 and 6, we note that both HIV exposure groups exhibit reduced FA in several overlapping tracts. Four connections with lower FA that included the left cerebral cortex were common between HIV exposure treatment groups.

HIV exposure initiation alters graph measures

In Table 7, the HEU_{pre} group of neonates had significantly lower efficiency in the basal ganglia (left putamen and right accumbens area) compared to HUU infants after multiple comparison correction.

We report in Table 7 that transitivity was significantly lower in the 4^{th} ventricle in the hindbrain in HEU_{post} compared to HUU neonates.

Associations between DTI tractography outcomes and maternal clinical outcomes

Among HIV-free infants exposed to HIV, we found no significant associations between maternal CD4 and DTI based measures (FA, MD and graph outcomes) in any of the affected tracts.

Discussion

Using DTI tractography, we identified neonatal white matter connections influenced by HIV and ART exposure duration in pregnancy in uninfected newborns. We found increased MD in white matter connections involving the thalamus and limbic system within HEU newborns who were exposed to ART since conception. Within the group of HEU neonates whose mothers initiated ART post conception, we observed reduced FA in cortical-subcortical as well as cerebellar connections. Overall, our analysis demonstrated distinct alterations in white matter properties related to the timing of maternal ART initiation that influence local brain network properties.

While the majority of results point to ART dependent differences in white matter development, we observed several connections across all HEU infants.

HIV exposure alters white matter integrity in tracts to the left cerebral cortex

We found four tracts in the left hemisphere with lower mean FA values across HEU ART groups compared to HUU infants. These tracts connect the left caudate, putamen, ventral diencephalon and midbrain to the left cerebral cortex, reflecting projection fibers vulnerable to intrauterine HIV exposure independent of maternal ART. Projection fibers connecting cortical and subcortical regions begin development during the second trimester around 17 weeks gestational age, becoming more massive and voluminous between 18 and 30 post conception weeks[47]. Axonal fasciculation is the process in which previously formed axons provide guidance for growing axons, with axons adhering to one another. This occurs during the third trimester and leads to bundles of axons that follow similar growth patterns[48]. As this occurs, the developing white matter becomes more anisotropic, resulting in increased FA and AD, and decreased RD, while MD remains unchanged[10]. As such, these tracts with lower FA and higher RD (uncorrected p-value) may represent less organized localized projection fibers in HEU infants compared to their HUU peers.

Within the imaging literature of HEU pediatric populations, altered white matter properties in projection fibers have been observed previously. Using voxelwise methods, Jankiewicz et al. reports higher FA in 7-year-old HEU children in a cluster in the right corona radiata[11], which connects the cerebral cortex to the thalamus and

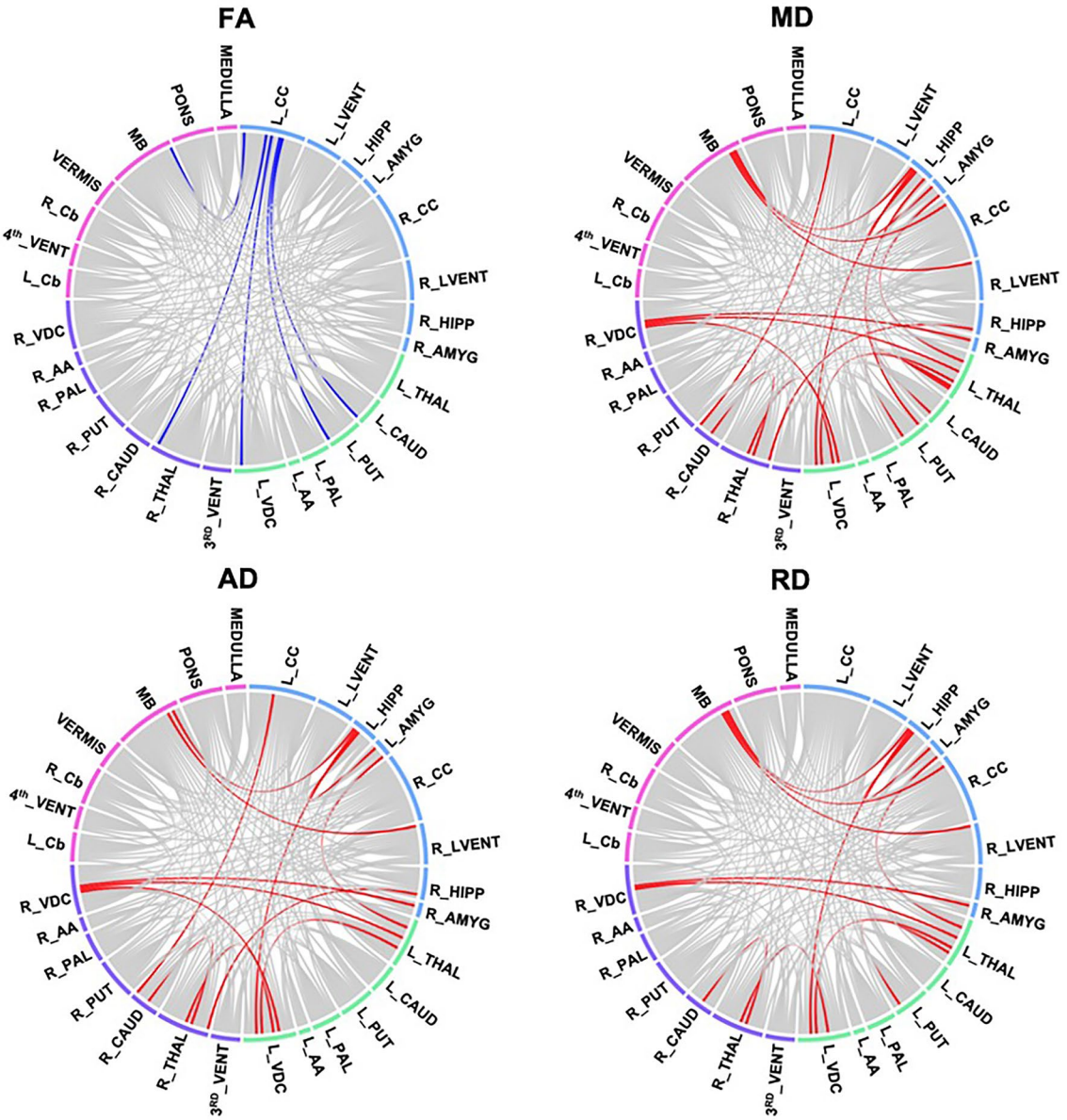

Figure 2. Chord diagram showing white matter connections with significant group differences in fractional anisotropy (FA), mean diffusivity (MD), axial diffusivity (AD) and radial diffusivity (RD) after FDR correction ($q < 0.05$) between HUU and HEU_{pre} infants. The colours correspond to the communities present in the modularity graph, which include the left and right basal ganglia (in green and purple respectively), the forebrain (in blue) and the hindbrain (in pink). *L/R, Left/Right. CC, Cerebral Cortex, LVENT, Lateral Ventricle; HIPP, Hippocampus; AMYG, Amygdala; THAL, Thalamus; CAUD, Caudate; PUT, Putamen; PAL, Pallidum; AA, Accumbens area; VDC, Ventral Diencephalon; 3rd VENT, 3rd Ventricle; Cb, Cerebellum; MB, Midbrain.

brainstem. While the direction of FA change and hemisphere are different than our findings, it is noteworthy that the same class of tracts is related to HIV-exposure in infancy and at 7-years.

Within this cohort, recently published work reported smaller left putamen volumes across all HEU infants, as well as smaller caudate volumes in infants whose mothers initiated ART post-conception[20]. The reported growth disruption of these structures may contribute to the observed white matter alterations, however further work is needed to demonstrate statistical links between these findings.

While we observed alterations in four tracts independent of ART initiation, the majority of our results involved distinct differences in relation to maternal treatment starting timing.

HEU infants demonstrated pre-myelination abnormalities despite early ART

We observed higher MD and RD/AD in HEU infants exposed to ART from conception compared to HUU infants, primarily in tracts that connect subcortical structures—only 2 of the 17 connections are to the cerebral cortex. Among the affected tracts, 8 involve the thalamus. The thalamus allows for communication between the

Connections	MD						AD						RD					
	Mean HUU (SD)	Mean HEU_{pre} (SD)	p	q	Std beta	Std error	Mean HUU (SD)	Mean HEU_{pre} (SD)	p	q	Std beta	Std error	Mean HUU (SD)	Mean HEU_{pre} (SD)	p	q	Std beta	Std error
L CC—R Caud	1.306 (0.048)	1.345 (0.057)	0.0011	0.026	0.432	0.141	1.660 (0.041)	1.703 (0.057)	0.0004	0.017	0.475	0.014	1.134 (0.055)	1.166 (0.060)	0.0095	0.057	0.344	0.134
L Thal—L Caud	1.219 (0.043)	1.247 (0.048)	0.0019	0.032	0.414	0.128	1.519 (0.063)	1.537 (0.059)	0.0526	0.138	0.260	0.016	1.076 (0.044)	1.099 (0.043)	0.0107	0.057	0.342	0.128
L Thal—L Put	1.211 (0.048)	1.242 (0.043)	0.0043	0.046	0.381	0.129	1.524 (0.062)	1.557 (0.054)	0.0103	0.057	0.345	0.016	1.055 (0.043)	1.081 (0.035)	0.0072	0.050	0.364	0.129
L Thal—L Amyg	1.293 (0.044)	1.345 (0.043)	0.0000	0.001	0.616	0.136	1.602 (0.053)	1.658 (0.058)	0.0001	0.012	0.549	0.016	1.145 (0.045)	1.189 (0.053)	0.0006	0.027	0.473	0.146
L Thal—L VDC	1.248 (0.046)	1.283 (0.041)	0.0004	0.016	0.487	0.123	1.572 (0.057)	1.607 (0.055)	0.0022	0.023	0.427	0.016	1.087 (0.035)	1.121 (0.041)	0.0002	0.012	0.496	0.135
L Thal—R VDC	1.277 (0.050)	1.303 (0.053)	0.0033	0.046	0.388	0.133	1.632 (0.086)	1.663 (0.063)	0.0041	0.032	0.383	0.019	1.100 (0.045)	1.126 (0.052)	0.0047	0.047	0.376	0.137
L Put—L Hipp	1.297 (0.078)	1.344 (0.046)	0.0042	0.046	0.390	0.189	1.650 (0.095)	1.694 (0.058)	0.0095	0.055	0.353	0.021	1.120 (0.072)	1.163 (0.052)	0.0182	0.070	0.318	0.148
L Hipp -L Amyg	1.319 (0.060)	1.389 (0.052)	0.0001	0.004	0.519	0.151	1.617 (0.093)	1.705 (0.077)	0.0005	0.017	0.456	0.024	1.175 (0.057)	1.230 (0.055)	0.0012	0.035	0.414	0.146
L Hipp—L VDC	1.377 (0.076)	1.429 (0.071)	0.0043	0.046	0.396	0.149	1.719 (0.102)	1.785 (0.068)	0.0016	0.020	0.443	0.024	1.195 (0.081)	1.250 (0.072)	0.0027	0.043	0.409	0.129
L Hipp—MB	1.363 (0.073)	1.416 (0.076)	0.0013	0.026	0.429	0.132	1.713 (0.101)	1.788 (0.105)	0.0020	0.023	0.413	0.028	1.187 (0.067)	1.231 (0.070)	0.0030	0.044	0.394	0.138
L VDC—R Thal	1.267 (0.043)	1.304 (0.043)	0.0007	0.025	0.444	0.128	1.629 (0.063)	1.668 (0.045)	0.0040	0.032	0.401	0.015	1.087 (0.034)	1.127 (0.041)	0.0000	0.003	0.524	0.132
L VDC—R VDC	1.278 (0.043)	1.319 (0.072)	0.0010	0.026	0.434	0.161	1.637 (0.068)	1.682 (0.073)	0.0014	0.020	0.427	0.019	1.105 (0.052)	1.130 (0.065)	0.0236	0.081	0.299	0.144
R CC—MB	1.306 (0.046)	1.341 (0.054)	0.0047	0.047	0.384	0.142	1.620 (0.062)	1.645 (0.059)	0.0681	0.169	0.250	0.016	1.153 (0.045)	1.190 (0.053)	0.0041	0.047	0.385	0.147
R LVent—MB	1.321 (0.057)	1.364 (0.055)	0.0040	0.046	0.385	0.150	1.673 (0.073)	1.731 (0.064)	0.0005	0.017	0.451	0.018	1.145 (0.056)	1.184 (0.054)	0.0070	0.050	0.361	0.150
R Thal—R Caud	1.216 (0.042)	1.256 (0.046)	0.0001	0.004	0.521	0.127	1.510 (0.055)	1.549 (0.055)	0.0006	0.017	0.451	0.014	1.070 (0.029)	1.106 (0.040)	0.0000	0.001	0.584	0.139
R Thal—R Hipp	1.372 (0.056)	1.406 (0.042)	0.0035	0.046	0.424	0.145	1.695 (0.063)	1.737 (0.051)	0.0006	0.017	0.490	0.016	1.211 (0.056)	1.240 (0.043)	0.0163	0.069	0.353	0.142
R Amyg—R VDC	1.321 (0.059)	1.359 (0.042)	0.0014	0.026	0.426	0.148	1.654 (0.067)	1.698 (0.055)	0.0030	0.028	0.398	0.017	1.155 (0.056)	1.190 (0.044)	0.0021	0.041	0.404	0.136

Table 5. Tracts showing higher mean diffusivity (MD) in infants in the HEU_{pre} group compared to those who are HUU after FDR correction ($q < 0.05$). Axial diffusivity (AD) and radial diffusivity (RD) in affected tracts are also shown. SD, standard deviation; L/R, Left/Right hemisphere. CC, Cerebral Cortex; Caud, Caudate; Thal, Thalamus; Put, Putamen; Amyg, Amygdala; VDC, Ventral Diencephalon; Hipp, Hippocampus; MB, Midbrain; LVent, Lateral Ventricle.

body and brain[49], relaying information and mediating the integration of information between specific cortical regions[50]. Once fiber bundles are organized pre-myelination occurs. During this period oligodendrocytes, glia cells that produce myelin, develop and mature. The process of oligodendroglial cell proliferation and development is isotropic, and is linked to decreased water and increased membrane density[51–53]. Taken together, this stage is characterized by constant FA and decreasing MD, RD and AD[10]. Our results in the pre-conception ART HEU group suggest pre-myelination in the affected tracts is hindered.

We find alterations in bilateral connections between the hippocampus, amygdala, thalamus and ventral diencephalon, which are part of the limbic system. These connections may belong to the fornix, a white matter component of the limbic system which connects the hippocampus to other subcortical structures in the limbic system. The fornix forms early, being visible in dissection studies by 13 weeks gestational age[54].

In addition, we report higher MD in connections between the thalamus and striatum, specifically to the caudate and putamen. The altered connections may be thalamic subcortical projections in the thalamostriatal pathway, a part of the cortico-striato-thalamo-cortical circuit, which has been associated with regions in the frontal cortex involved in sensorimotor, limbic and cognitive information processing[50].

In our cohort, the pre-conception HEU neonates were exposed to intrauterine ART during the first trimester as compared to the post-conception group. The most reported in utero ART effect on the brain is mitochondrial dysfunction[55] and points to postponed pre-myelination in the affected tracts caused by decreased cellular metabolism[56]. Mitochondria are involved in creating cellular energy and mitochondrial disorder presents with a variety of neurological effects in infants and children. Our findings of higher MD in the pre-conception group suggest an ART effect on pre-myelinated white matter to/from the thalamus. However, further work is needed to link these alterations to mitochondrial dysfunction.

Connections	FA						AD						RD					
	Mean HUU (SD)	Mean HEU_{post} (SD)	p	q	Std beta	Std error	Mean HUU (SD)	Mean HEU_{post} (SD)	p	q	Std beta	std error	Mean HUU (SD)	Mean HEU_{post} (SD)	p	q	Std beta	Std error
L CC—L Thal	0.209 (0.011)	0.200 (0.010)	0.0015	0.024	− 0.413	0.003	1.635 (0.067)	1.652 (0.071)	0.530	0.993	0.083	0.018	1.190 (0.061)	1.218 (0.048)	0.143	0.348	0.192	0.014
L CC—L Caud	0.221 (0.007)	0.213 (0.011)	0.0013	0.024	− 0.436	0.003	1.633 (0.069)	1.646 (0.067)	0.583	0.993	0.074	0.018	1.172 (0.057)	1.188 (0.050)	0.261	0.439	0.150	0.014
L CC—L Put	0.208 (0.008)	0.198 (0.008)	0.0001	0.010	− 0.542	0.002	1.605 (0.063)	1.625 (0.065)	0.392	0.993	0.114	0.017	1.172 (0.060)	1.194 (0.056)	0.174	0.365	0.177	0.015
L CC—L Pal	0.224 (0.009)	0.217 (0.010)	0.0066	0.048	− 0.372	0.003	1.620 (0.067)	1.630 (0.063)	0.638	0.993	0.063	0.017	1.152 (0.056)	1.176 (0.059)	0.123	0.328	0.201	0.015
L CC—L Amyg	0.220 (0.013)	0.210 (0.013)	0.0018	0.026	− 0.432	0.004	1.693 (0.058)	1.709 (0.093)	0.824	0.993	0.030	0.020	1.205 (0.054)	1.236 (0.056)	0.087	0.287	0.216	0.014
L CC—L VDC	0.224 (0.009)	0.215 (0.006)	0.0000	0.000	− 0.642	0.002	1.648 (0.069)	1.658 (0.075)	0.778	0.993	0.038	0.019	1.173 (0.058)	1.192 (0.056)	0.295	0.469	0.139	0.015
L CC—R CC	0.195 (0.008)	0.189 (0.005)	0.0075	0.048	− 0.372	0.002	1.620 (0.072)	1.641 (0.054)	0.286	0.993	0.140	0.017	1.208 (0.063)	1.235 (0.047)	0.038	0.265	0.272	0.014
LCC—R LVent	0.227 (0.009)	0.221 (0.010)	0.0057	0.048	− 0.376	0.002	1.742 (0.097)	1.756 (0.090)	0.809	0.993	0.032	0.025	1.227 (0.074)	1.251 (0.064)	0.306	0.477	0.139	0.019
L CC—MB	0.225 (0.007)	0.215 (0.010)	0.0007	0.023	− 0.474	0.003	1.632 (0.062)	1.637 (0.070)	0.918	0.993	− 0.014	0.018	1.156 (0.050)	1.184 (0.045)	0.061	0.274	0.246	0.013
L CC—Pons	0.224 (0.009)	0.216 (0.010)	0.0063	0.048	− 0.387	0.003	1.641 (0.067)	1.652 (0.058)	0.769	0.993	0.040	0.017	1.170 (0.055)	1.199 (0.042)	0.052	0.274	0.262	0.013
L Cb—R CC	0.179 (0.015)	0.168 (0.010)	0.0015	0.024	− 0.409	0.003	1.474 (0.079)	1.476 (0.082)	0.818	0.993	0.031	0.021	1.119 (0.066)	1.152 (0.086)	0.092	0.287	0.226	0.020
L Cb—4th Vent	0.234 (0.011)	0.223 (0.011)	0.0011	0.023	− 0.457	0.003	1.596 (0.052)	1.611 (0.065)	0.662	0.993	0.058	0.015	1.106 (0.049)	1.144 (0.052)	0.008	0.250	0.339	0.013
L Cb—R Cb	0.174 (0.016)	0.162 (0.009)	0.0004	0.023	− 0.471	0.004	1.427 (0.050)	1.424 (0.043)	0.826	0.993	− 0.032	0.013	1.085 (0.058)	1.111 (0.035)	0.040	0.265	0.285	0.013
L Cb—Pons	0.185 (0.017)	0.172 (0.015)	0.0008	0.023	− 0.437	0.004	1.497 (0.073)	1.522 (0.089)	0.277	0.993	0.146	0.022	1.130 (0.068)	1.174 (0.084)	0.022	0.250	0.300	0.020
L Cb—Medulla	0.189 (0.019)	0.176 (0.021)	0.0021	0.028	− 0.401	0.005	1.501 (0.095)	1.534 (0.105)	0.201	0.979	0.170	0.026	1.125 (0.092)	1.169 (0.092)	0.058	0.274	0.251	0.024
4th Vent—R CC	0.243 (0.020)	0.231 (0.012)	0.0078	0.048	− 0.355	0.005	1.595 (0.069)	1.604 (0.047)	0.542	0.993	0.081	0.015	1.100 (0.062)	1.126 (0.040)	0.062	0.274	0.244	0.014
4th Vent—Pons	0.210 (0.024)	0.198 (0.017)	0.0078	0.048	− 0.357	0.006	1.570 (0.094)	1.571 (0.097)	0.973	0.993	− 0.004	0.025	1.139 (0.073)	1.175 (0.084)	0.080	0.287	0.228	0.020
4th Vent—Medulla	0.193 (0.026)	0.173 (0.019)	0.0031	0.034	− 0.382	0.006	1.55 (0.110)	1.583 (0.112)	0.449	0.993	0.100	0.029	1.157 (0.094)	1.220 (0.102)	0.025	0.250	0.290	0.026
R CC—R Cb	0.201 (0.010)	0.193 (0.011)	0.0038	0.038	− 0.401	0.003	1.577 (0.053)	1.577 (0.051)	0.789	0.993	− 0.037	0.014	1.150 (0.049)	1.176 (0.043)	0.055	0.274	0.241	0.012
R CC—R Thal	0.207 (0.009)	0.200 (0.009)	0.0056	0.048	− 0.372	0.002	1.624 (0.063)	1.634 (0.065)	0.930	0.993	0.011	0.016	1.187 (0.058)	1.203 (0.057)	0.447	0.581	0.096	0.014
R CC—R Put	0.205 (0.011)	0.198 (0.007)	0.0067	0.048	− 0.355	0.002	1.589 (0.057)	1.599 (0.056)	0.723	0.993	0.047	0.015	1.161 (0.058)	1.174 (0.055)	0.433	0.571	0.101	0.014
R CC—R VDC	0.218 (0.013)	0.210 (0.007)	0.0074	0.048	− 0.356	0.003	1.640 (0.062)	1.652 (0.055)	0.615	0.993	0.069	0.016	1.169 (0.055)	1.196 (0.058)	0.153	0.361	0.189	0.015
R Cb—Vermis	0.168 (0.015)	0.160 (0.008)	0.0067	0.048	− 0.372	0.004	1.403 (0.067)	1.398 (0.067)	0.535	0.993	− 0.084	0.018	1.083 (0.052)	1.090 (0.043)	0.670	0.776	0.057	0.013
R Cb—MB	0.193 (0.017)	0.185 (0.015)	0.0073	0.048	− 0.357	0.004	1.475 (0.047)	1.472 (0.071)	0.408	0.993	− 0.111	0.016	1.097 (0.053)	1.106 (0.044)	0.669	0.776	0.057	0.013
R Cb—Medulla	0.188 (0.021)	0.173 (0.013)	0.0010	0.023	− 0.435	0.005	1.478 (0.077)	1.501 (0.086)	0.350	0.993	0.124	0.021	1.120 (0.084)	1.149 (0.060)	0.080	0.287	0.236	0.020
R Put—Pons	0.251 (0.012)	0.240 (0.015)	0.0026	0.032	− 0.422	0.004	1.574 (0.055)	1.559 (0.058)	0.251	0.993	− 0.162	0.016	1.076 (0.046)	1.077 (0.040)	0.937	0.959	− 0.011	0.012
Vermis—Pons	0.187 (0.016)	0.177 (0.013)	0.0029	0.033	− 0.392	0.004	1.484 (0.056)	1.496 (0.090)	0.952	0.993	− 0.008	0.020	1.108 (0.050)	1.139 (0.066)	0.070	0.274	0.232	0.015
Vermis—Medulla	0.186 (0.025)	0.172 (0.013)	0.0010	0.023	− 0.434	0.005	1.472 (0.103)	1.483 (0.099)	0.985	0.997	− 0.003	0.027	1.102 (0.086)	1.134 (0.080)	0.122	0.328	0.212	0.022

Table 6. Tracts where infants in the HEU_{post} group have lower (FDR $q < 0.05$) fractional anisotropy (FA) than those who are HUU. Axial diffusivity (AD) and radial diffusivity (RD) in affected tracts are also shown. SD, standard deviation; L/R, Left/Right hemisphere. CC, Cerebral Cortex; Thal, Thalamus; Caud, Caudate; Put, Putamen; Pal, Pallidum; Amyg, Amygdala; VDC, Ventral Diencephalon; LVent, Lateral Ventricle; MB, Midbrain; Cb, Cerebellum; 4th Vent, 4th Ventricle.

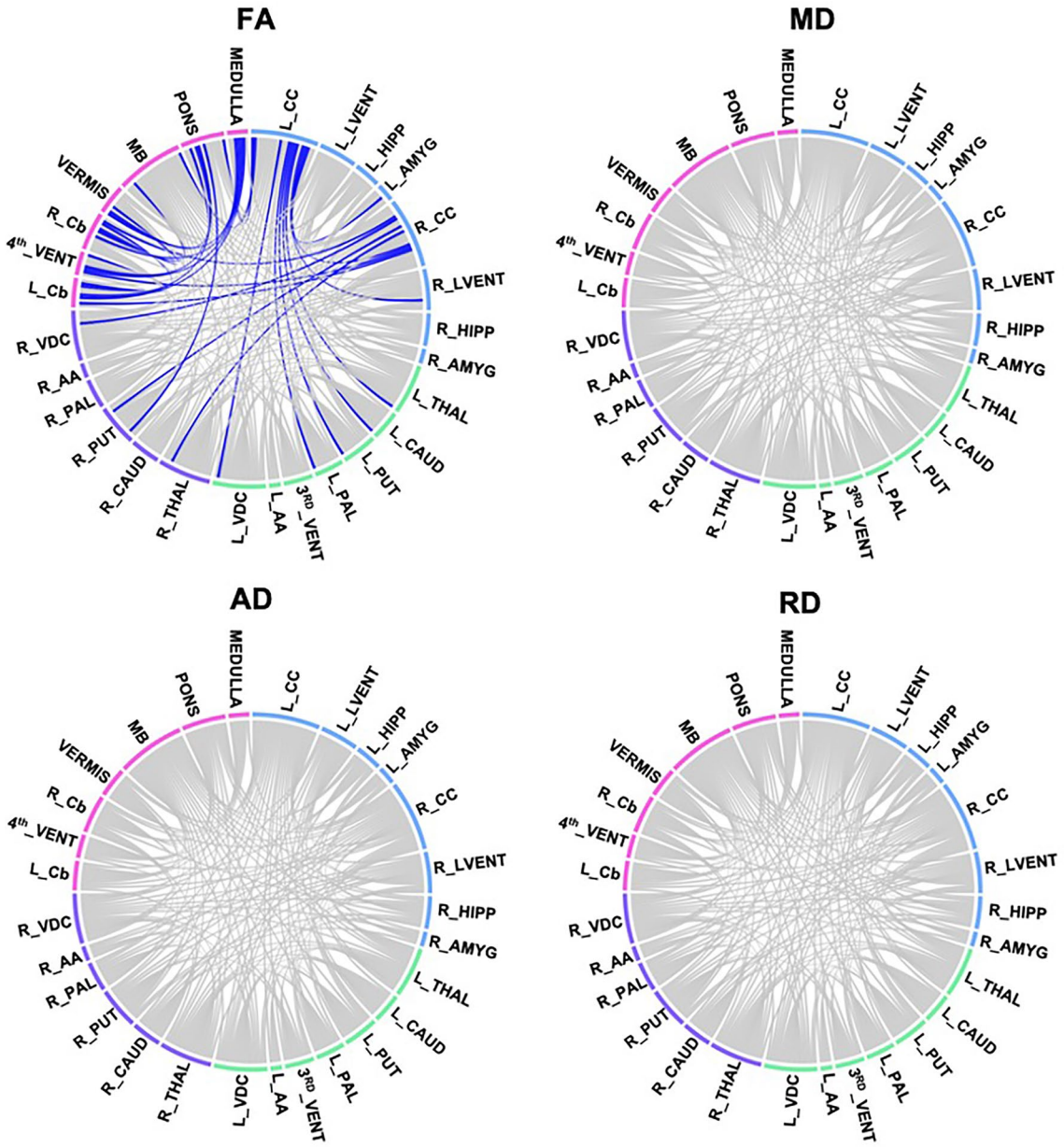

Figure 3. Chord diagram showing WM connections with significant group differences in fractional anisotropy (FA), mean diffusivity (MD), axial diffusivity (AD) and radial diffusivity (RD) after FDR correction ($q < 0.05$) between HUU and HEU_{post} infants. The colours correspond to the communities present in the modularity graph, which include the left and right basal ganglia (in green and purple respectively), the forebrain (in blue) and the hindbrain (in pink). *L/R, Left/Right. CC, Cerebral Cortex; LVENT, Lateral Ventricle; HIPP, Hippocampus; AMYG, Amygdala; THAL, Thalamus; CAUD, Caudate; PUT, Putamen; PAL, Pallidum; AA, Accumbens area; VDC, Ventral Diencephalon; 3rd VENT, 3rd Ventricle; Cb, Cerebellum; MB, Midbra.

Among the pre-conception ART HEU group, graph analysis found lower nodal efficiency in the left putamen and right accumbens areas. Nodal efficiency is a measure of integration, estimating the ability to send information between grey matter seeds and network nodes[36,57]. The striatum plays an important role in facilitating information transfer between the cortex and thalamus. Our results suggest that altered subcortical white matter integrity, in the form of higher MD, AD, and RD, influences information processing in the basal ganglia community.

When comparing the post-conception HEU group to the control infant group, we identified differences in DTI parameters across various tracts as well as graph metrics.

Post-conception ART exposure affects white matter development in the hindbrain

In comparison to HUU newborns, connections with lower FA among newborns exposed to ART post-conception primarily involved cortical-subcortical as well as cerebellar connections. The cortical-subcortical tracts, like those also discussed in relation to the HIV-exposure, are projection fibers which begin development during the second

HUU vs HEU_{pre}						
Nodal efficiency						
Region name	**Mean HUU (SD)**	**Mean HEU_{pre} (SD)**	**p**	**q**	**Std beta**	**Std error**
L Put	2590 (2393)	1186 (475)	0.002	0.034	− 0.454	0.139
R AA	2697 (1903)	2431 (2013)	0.002	0.034	− 0.441	0.139
HUU vs HEU_{post}						
Transitivity						
Region name	**Mean HUU (SD)**	**Mean HEU_{post} (SD)**	**p**	**q**	**Std beta**	**Std error**
4th Vent	0.948 (0.012)	0.939 (0.006)	0.001	0.012	− 0.462	0.126

Table 7. Graph theory measures with significant group differences after FDR correction ($q < 0.05$). L/R, Left/Right; Put, Putamen; AA, Accumbens area; 4th Vent, 4th Ventricle.

trimester (13–28 weeks). This falls in the timeframe when mothers living with HIV in the post-conception group initiated treatment, 14–36 weeks post conception. The formation of axonal pathways takes place primarily after neuronal migration midway through pregnancy, and by birth at full term all major fibers are established[8]. As a result, growing axonal pathways are vulnerable during this period. The lower FA in these tracts may represent delayed axonal bundle organization due to maternal HIV disruptions to the fetal environment before ART was initiated.

Half of the connections with reduced FA in the post-conception ART HEU group involved the cerebellum and/or the brainstem. Coherent pathways of the cerebellar peduncles have been observed as early as 17 weeks gestational age[58]. Among voxelwise DTI studies in HEU infants and children, altered FA has been previously reported in the hindbrain. A study in newborns found increased FA in the cerebellar peduncles[15], while a study in 10-year-old children reported decreased FA in the posterior cerebellum[12]. Taken together, our findings and the literature provide evidence that this region is vulnerable to maternal HIV exposure in infancy and early childhood.

Unlike the pre-conception ART exposure group, we observed reduced FA between the left and right cerebral cortex in infants exposed to ART in utero post conception. The pioneering axons of the corpus callosum, the largest set of commissural fibers, form around 13 gestational weeks[59,60]. From 13 to 23 weeks, fibers develop in an antero-posterior direction until the callosal fibers become uniform[54]. This window represents the period when mothers in this group were initiating ART. In the pre-conception group, ART may have protected the early development of the corpus callosum.

In terms of network measures, we observed lower transitivity around the 4th ventricle of newborns whose mothers living with HIV initiated ART post conception as compared to the HUU group. The 4th ventricle sits between the pons, medulla oblongata and cerebellum. The observed tracts involving the 4th ventricle likely represent an adjacent structure(s) connected via the cerebellar peduncles. Transitivity is a measure of segregation related to specialized processing[57]. As compared to the HUU group, reduced transitivity may disrupt the development of specific domains within the interconnected hindbrain community structures. Considering the majority of tracts in the post-conception ART HEU group demonstrated lower FA in comparison to the HUU group in the hindbrain, these changes may contribute to the observed reduced transitivity.

The distinct outcomes based on ART initiation timing suggests exposure to treatment plays a role in the alterations reported in HEU infants and children. These results highlight the importance of including maternal ART data into studies of neurodevelopment in HEU populations.

Limitations

Due to the increasing availability and access to treatment, and the benefits of ART to both the mother and infant, we do not include a comparison between mothers living with HIV not on ART. The conclusions drawn from this study can only inform discussions relating to the initiation of treatment in mothers living with HIV.

The white matter connections identified in this study are influenced by the size and number of seeds used for analysis. The Infant Freesurfer tool was used for segmentation, and the cortex is not subdivided into lobes or smaller divisions. As a result, the conclusions we can draw regarding connections to and within specific cortical regions are limited.

The DTI measures presented are derived from analysis based on several initial assumptions and are sensitive to methodological procedure[61]. Acquisition parameters, pre-processing steps, reconstruction/propagation models, and statistical analysis all affect the final sensitivity, specificity, and accuracy of a study[61,62].

Conclusions and future work

Using DTI tractography, we identified distinctive alterations in structural integrity and connectome measures in HEU infants related to maternal ART initiation. HEU newborns exposed to ART since conception demonstrated higher MD, RD and AD in connections between subcortical structures, many involving the thalamus. These changes suggest regional delayed pre-myelination. Further, reduced nodal efficiency in the striatum suggests altered subcortical white matter integrity influences the integration of information in the basal ganglia community. Within HEU newborns exposed to ART post-conception, we observed lower FA in cortical-subcortical and hindbrain connections, suggesting delays in axonal organization. In conjunction, we reported reduced transitivity

in the hindbrain community which may influence regional functional processing. The initiation of ART before conception may have protected early white matter development in the hindbrain.

A recent meta-analysis of neurodevelopment outcomes in HEU infants found a risk of impairment in expressive language and gross motor development by age 2 years[5]. The predominant regions affected in both ART exposure groups, the thalamus, striatum, and cerebellum, are involved in aspects of language and motor development. The thalamus includes nuclei involved in motor activity, which relay and integrate information between the cortex and the basal ganglia or cerebellum[63]. Through the functional cortico-striato-thalamocortical neural pathways, the striatum is involved in the learning of motor skills[64]. The basal ganglia have been implicated in learning language, with basal ganglia abnormalities related to developmental disorders of language[65]. And, while it is well established that the cerebellum is involved in motor function, it also plays a role in various brain functions such as language, visuospatial ability and attention[66–69]. As a result, the reported abnormalities may contribute to later neurodevelopmental delays in language and motor domains in these infants. Further work is needed to explore whether our findings at the white matter connection or network level contribute to cognitive deficits in this cohort.

Data availability

The datasets generated during and/or analysed during the current study are available from the corresponding author upon reasonable request.

Received: 11 July 2023; Accepted: 27 March 2024
Published online: 17 April 2024

References

1. Dreier, J. W., Andersen, A. M. N. & Berg-Beckhoff, G. Systematic review and meta-analyses: fever in pregnancy and health impacts in the offspring. *Pediatrics.* **133** (2014).
2. Racicot, K. & Mor, G. Risks associated with viral infections during pregnancy. *J. Clin. Investig.* **127**, 1591–1599 (2017).
3. Hickey, M. K. *et al.* Infants exposed to antibiotics after birth have altered recognition memory responses at one month of age. *Pediatr. Res.* **89**, 1500–1507 (2020).
4. Auriti, C. *et al.* Pregnancy and viral infections: Mechanisms of fetal damage, diagnosis and prevention of neonatal adverse outcomes from cytomegalovirus to SARS-CoV-2 and Zika virus. *Biochim. Biophys. Acta Mol. Basis Dis.* **1867**, 456 (2021).
5. Wedderburn, C. J. *et al.* Early structural brain development in infants exposed to HIV and antiretroviral therapy *in utero* in a South African birth cohort. *J. Int. AIDS Soc.* **25**, 1 (2022).
6. Girault, J. B. *et al.* White matter connectomes at birth accurately predict cognitive abilities at age 2. *Neuroimage* https://doi.org/10.1016/j.neuroimage.2019.02.060 (2019).
7. Hüppi, P. S. *et al.* Quantitative magnetic resonance imaging of brain development in premature and mature newborns. *Ann. Neurol.* **43**, 224–235 (1998).
8. Dubois, J. *et al.* The early development of brain white matter: A review of imaging studies in fetuses, newborns and infants. *Neuroscience* **276**, 48–71 (2014).
9. Ball, G. *et al.* Rich-club organization of the newborn human brain. *Proc. Natl. Acad. Sci. U. S. A.* **111**, 7456–7461 (2014).
10. Dubois, J. *et al.* Asynchrony of the early maturation of white matter bundles in healthy infants: Quantitative landmarks revealed noninvasively by diffusion tensor imaging. *Hum. Brain Mapp.* **29**, 14 (2008).
11. Jankiewicz, M. *et al.* White matter abnormalities in children with HIV infection and exposure. *Front. Neuroanat.* **11**, 1–9 (2017).
12. Yadav, S. K. *et al.* Brain microstructural changes support cognitive deficits in HIV uninfected children born to HIV infected mothers. *Brain Behav. Immun. Health* **2**, 100039 (2020).
13. Madzime, J. *et al.* Altered white matter tracts in the somatosensory, salience, motor, and default mode networks in 7-year-old children living with human immunodeficiency virus: A tractographic analysis. *Brain Connect* **12**, 302–319 (2022).
14. Jahanshad, N. *et al.* Brain imaging and neurodevelopment in HIV-uninfected Thai children born to HIV-infected mothers. *Pediatr. Infect. Dis. J.* **34**, e211 (2015).
15. Tran, L. T. *et al.* White matter microstructural integrity and neurobehavioral outcome of HIV-exposed uninfected neonates. *Medicine* **95**, 2577 (2016).
16. Jacobson, S. W., Chiodo, L. M., Sokol, R. J. & Jacobson, J. L. Validity of maternal report of prenatal alcohol, cocaine, and smoking in relation to neurobehavioral outcome. *Pediatrics* **109**, 815–825 (2002).
17. Dodge, N. C. *et al.* Prenatal alcohol exposure and interhemispheric transfer of tactile information: Detroit and Cape Town findings. *Alcohol Clin. Exp. Res.* **33**, 1628–1637 (2009).
18. Pettker, C. M., Goldberg, J. D., El-Sayed, Y. Y. & Copel, J. A. Methods for estimating the due date. *Obstetr. Gynecol.* **129**, 967–968 (2017).
19. National Department of Health, Republic of South Africa. *Guidelines for Maternity Care in South Africa. A Manual for Clinics, Community Health Centres and District Hospitals.* https://knowledgehub.health.gov.za/elibrary/guidelines-maternity-care-south-africa-2016 (2016).
20. Ibrahim, A. *et al.* Maternal ART throughout gestation prevents caudate volume reductions in neonates who are HIV exposed but uninfected. *Front. Neurosci.* **17**, 456 (2023).
21. Setsompop, K. *et al.* Improving diffusion MRI using simultaneous multi-slice echo planar imaging. *Neuroimage* **63**, 569 (2012).
22. Cox, R. W. AFNI: Software for analysis and visualization of functional magnetic resonance neuroimages. *Comput. Biomed. Res.* **29**, 162–173 (1996).
23. Pierpaoli, C. *et al.* TORTOISE: An integrated software package for processing of diffusion MRI data. In *ISMRM 18th annual meeting* (2010).
24. Zöllei, L., Iglesias, J. E., Ou, Y., Grant, P. E. & Fischl, B. Infant FreeSurfer: An automated segmentation and surface extraction pipeline for T1-weighted neuroimaging data of infants 0–2 years. *Neuroimage* **218**, 116946 (2020).
25. Taylor, P. A. & Saad, Z. S. FATCAT: (An efficient) functional and tractographic connectivity analysis toolbox. *Brain Connect* **3**, 523 (2013).
26. Irfanoglu, M. O. *et al.* DR-BUDDI (diffeomorphic registration for blip-up blip-down diffusion imaging) method for correcting echo planar imaging distortions. *Neuroimage* **106**, 284 (2015).
27. de Macedo Rodrigues, K. *et al.* A FreeSurfer-compliant consistent manual segmentation of infant brains spanning the 0–2 year age range. *Front. Hum. Neurosci.* **9**, 21 (2015).
28. Curran, K. M., Emsell, L. & Leemans, A. *Quantitative DTI Measures. Diffusion Tensor Imaging: A Practical Handbook* 6587 (Springer, 2016). https://doi.org/10.1007/978-1-4939-3118-7_5.

29. Soares, J. M., Marques, P., Alves, V. & Sousa, N. A hitchhiker's guide to diffusion tensor imaging. *Front. Neurosci.* **7**, 31 (2013).
30. Lebel, C. *et al.* Diffusion tensor imaging of white matter tract evolution over the lifespan. *Neuroimage* **60**, 340–352 (2012).
31. Tian, L. & Ma, L. Microstructural changes of the human brain from early to mid-adulthood. *Front. Hum. Neurosci.* **11**, 393 (2017).
32. Taylor, P. A., Chen, G., Cox, R. W. & Saad, Z. S. Open environment for multimodal interactive connectivity visualization and analysis. *Brain Connect* **6**, 109 (2016).
33. Dubois, J., Hertz-Pannier, L., Dehaene-Lambertz, G., Cointepas, Y. & Le Bihan, D. Assessment of the early organization and maturation of infants' cerebral white matter fiber bundles: A feasibility study using quantitative diffusion tensor imaging and tractography. *Neuroimage* **30**, 1121–1132 (2006).
34. Kasprian, G. *et al.* In utero tractography of fetal white matter development. *Neuroimage* **43**, 213–224 (2008).
35. R Core Team. *R: A Language and Environment for Statistical Computing.* R Foundation for Statistical Computing. https://www.R-project.org/ (Vienna, Austria, 2020).
36. Griffa, A., Baumann, P. S., Thiran, J. P. & Hagmann, P. Structural connectomics in brain diseases. *Neuroimage* **80**, 515–526 (2013).
37. Caeyenberghs, K. *et al.* Brain connectivity and postural control in young traumatic brain injury patients: A diffusion MRI based network analysis. *Neuroimage Clin.* **1**, 106–115 (2012).
38. Watson, C. G., DeMaster, D. & Ewing-Cobbs, L. Graph theory analysis of DTI tractography in children with traumatic injury. *Neuroimage Clin.* **21**, 101673 (2019).
39. Kim, M. S., An, M. H., Kim, W. J. & Hwang, T. H. Comparative efficacy and safety of pharmacological interventions for the treatment of COVID-19: A systematic review and network meta-analysis. *PLoS Med.* **17**, 1003 (2020).
40. Mijalkov, M., Kakaei, E., Pereira, J. B., Westman, E. & Volpe, G. BRAPH: A graph theory software for the analysis of brain connectivity. *PLoS One* **12**, e0178798 (2017).
41. Rodrigue, J.-P. The geography of transport systems. *Geogr. Transp. Syst.* https://doi.org/10.4324/9780429346323 (2020).
42. Luo, W., Greene, A. S. & Constable, R. T. Within node connectivity changes, not simply edge changes, influence graph theory measures in functional connectivity studies of the brain. *Neuroimage* **240**, 118332 (2021).
43. Kocevar, G. *et al.* Graph theory-based brain connectivity for automatic classification of multiple sclerosis clinical courses. *Front. Neurosci.* **10**, 478 (2016).
44. Ma, X. *et al.* Enhanced network efficiency of functional brain networks in primary insomnia patients. *Front. Psychiatry* **9**, 145 (2018).
45. Kim, E. *et al.* Morphological brain network assessed using graph theory and network filtration in deaf adults. *Hear. Res.* **315**, 88–98 (2014).
46. Latora, V. & Marchiori, M. Efficient behavior of small-world networks. *Phys. Rev. Lett.* **87**, 198701 (2001).
47. Vasung, L., Raguz, M., Kostovic, I. & Takahashi, E. Spatiotemporal relationship of brain pathways during human fetal development using high-angular resolution diffusion MR imaging and histology. *Front. Neurosci.* **11**, 348 (2017).
48. Kostović, I. & Jovanov-Milošević, N. The development of cerebral connections during the first 20–45 weeks' gestation. *Semin. Fetal. Neonatal. Med.* **11**, 415–422 (2006).
49. Torrico, T. J. & Munakomi, S. Neuroanatom, Thalamus. *StatPearls* **2021**, 485 (2021).
50. Draganski, B. *et al.* Evidence for segregated and integrative connectivity patterns in the human Basal Ganglia. *J. Neurosci.* **28**, 7143–7152 (2008).
51. Prayer, D. *et al.* Visualization of nonstructural changes in early white matter development on diffusion-weighted MR images: Evidence supporting premyelination anisotropy. *AJNR Am. J. Neuroradiol.* **22**, 1572 (2001).
52. Wimberger, D. M. *et al.* Identification of 'premyelination' by diffusion-weighted MRI. *J. Comput. Assist. Tomogr.* **19**, 28–33 (1995).
53. Baumann, N. & Pham-Dinh, D. Biology of oligodendrocyte and myelin in the mammalian central nervous system. *Physiol. Rev.* **81**, 871–927 (2001).
54. Horgos, B. *et al.* White matter dissection of the fetal brain. *Front. Neuroanat.* **2020**, 14 (2020).
55. Schnoll, J. G. *et al.* Evaluating neurodevelopmental consequences of perinatal exposure to antiretroviral drugs: Current challenges and new approaches. *J. Neuroimmune Pharmacol.* **16**, 113–129 (2021).
56. Gropman, A. L. Neuroimaging in mitochondrial disorders. *Neurotherapeutics* **10**, 273 (2013).
57. Rubinov, M. & Sporns, O. Complex network measures of brain connectivity: Uses and interpretations. *Neuroimage* **52**, 1059–1069 (2010).
58. Takahashi, E., Hayashi, E., Schmahmann, J. D. & Ellen-Grant, P. Development of cerebellar connectivity in human fetal brains revealed by high angular resolution diffusion tractography. *Neuroimage* **96**, 326–333 (2014).
59. Rakic, P. & Yakovlev, P. I. Development of the corpus callosum and cavum septi in man. *J. Comp. Neurol.* **132**, 45–72 (1968).
60. Ren, T. *et al.* Imaging, anatomical, and molecular analysis of callosal formation in the developing human fetal brain. *Anat. Rec. A Discov. Mol. Cell Evol. Biol.* **288**, 191–204 (2006).
61. Campbell, J. S. W. & Pike, G. B. Potential and limitations of diffusion MRI tractography for the study of language. *Brain Lang.* **131**, 65–73 (2014).
62. Jones, D. K. & Cercignani, M. Twenty-five pitfalls in the analysis of diffusion MRI data. *NMR Biomed.* **23**, 803–820 (2010).
63. Bosch-Bouju, C., Hyland, B. I. & Parr-Brownlie, L. C. Motor thalamus integration of cortical, cerebellar and basal ganglia information: Implications for normal and parkinsonian conditions. *Front. Comput. Neurosci.* **7**, 145 (2013).
64. Grohs, M. N., Lebel, C., Carlson, H. L., Craig, B. T. & Dewey, D. Subcortical brain structure in children with developmental coordination disorder: A T1-weighted volumetric study. *Brain Imaging Behav.* **15**, 2756–2765 (2021).
65. Ullman, M. T., Earle, F. S., Walenski, M. & Janacsek, K. The neurocognition of developmental disorders of language. *Annu. Rev. Psychol.* **71**, 389–417 (2020).
66. Mariën, P. *et al.* Consensus paper: Language and the cerebellum: An ongoing enigma. *Cerebellum* **13**, 386–410 (2014).
67. Mariën, P. & Borgatti, R. Language and the cerebellum. *Handb. Clin. Neurol.* **154**, 181–202 (2018).
68. Molinari, M. *et al.* Cerebellum and procedural learning: Evidence from focal cerebellar lesions. *Brain* **120**(Pt 10), 1753–1762 (1997).
69. Riva, D. The cerebellar contribution to language and sequential functions: Evidence from a child with cerebellitis. *Cortex* **34**, 279–287 (1998).

Author contributions

NM: data analysis, interpretation of results, figure creation, drafting and review of manuscript. MH: oversight, project design, data analysis, interpretation of results, drafting and review of manuscript. EM: conception and design of study, study oversight, data acquisition, review of manuscript. FLW: data curation and review of manuscript. FL: review of manuscript. AvdK: conception and design of study, study oversight, data acquisition and review of manuscript. BL: conception and design of study, study oversight, data acquisition and curation, and review of manuscript. MJ: oversight, project design, data analysis, interpretation of results, and review of manuscript.

Funding
This work was funded by National Institutes of Health (NIH) Grants R01-HD085813 (BL, EM, and AvdK) and R01-HD093578 (MH, AvdK, and Kaba).

Competing interests
The authors declare no competing interests.

Additional information
Correspondence and requests for materials should be addressed to N.M. or E.M.M.

Reprints and permissions information is available at www.nature.com/reprints.

Publisher's note Springer Nature remains neutral with regard to jurisdictional claims in published maps and institutional affiliations.